Flight Dynamics of a Coaxial Compound Helicopter with Rotor-On-Rotor Interactional Aerodynamics

Dogyu Jun
Graduate Research Assistant
Alessandro Cocco
Postdoctoral Researcher
Umberto Saetti
Assistant Professor
Department of Aerospace Engineering
University of Maryland
College Park, MD 20740

Ondrej Juhasz
Assistant Professor
United States Naval Academy
Annapolis, MD 21402

ABSTRACT

This paper focuses on the integration of a generalized rotor-on-rotor interactional aerodynamics model in state-variable form within a flight dynamics simulation and on its subsequent linearization and linear model analysis. The aircraft chosen for this investigation is a generic lift-offset compound coaxial rotorcraft. Upon trimming the flight dynamics at hover, linearized models of the dynamics are compared to nonlinear simulations, and with baseline models that do not account for rotor-on-rotor inflow interference effects. Model-order reduction methods are investigated to guide the development of linearized models that are tractable for flight control design while still predicting the effect of rotor-on-rotor interactions on the vehicle flight dynamics. It is found that, at hover and for the coaxial configuration in consideration, rotor-on-rotor interactions result in a lower magnitude of the rolling/pitching moment to lateral/longitudinal velocity derivative and in a lower roll/pitch damping derivative. These changes in stability derivatives yield roll and pitch subsidence modes at a lower frequency and roll and pitch oscillation modes with a higher natural frequency. The resulting frequency responses show a reduction in the magnitude of the roll response to on axis inputs (approximately 0.7 to 10 rad/s). In forward flight, the dominant effect is at low frequencies in the pitch axis. These findings are in line with previous studies focusing on flight-test data based model validation of the Sikorsky X2TD$^{\text{TM}}$.

INTRODUCTION

Future Vertical Lift (FVL) vehicles feature multiple rotors, rigid rotor systems, and high levels of aerodynamic interactions. These features drive the need for advanced aeromechanics models while at the same time making real-time speeds (or even sufficiently fast execution speeds for routine design) much more difficult. Using high-fidelity CFD or mid-fidelity vortex wake methods for modeling aerodynamic interactions and multiple rotors requires larger amounts of wake data to be computed, and rigid rotor systems require costly structural dynamics models of the blades. Thus, while more advanced aeromechanics models are feasible, it is likely that in many cases, execution speeds required for real-time simulations or routine design applications will remain elusive. Additionally, validation of the dynamic response of these high-order models is often incomplete or lacking.

There is also an increasing need for advanced models to be capable of fast prediction of the rotor-on-rotor interactional aerodynamics rotor loads to determine flight dynamics characteristics and for rapid evaluation of advanced control architectures. It is therefore critical that high fidelity aeromechanics models are formulated in such a way that they can be readily linearized and/or simplified to extract more tractable and less expensive models. Not only are linearized models used in most practical control design methodologies, but linear model analysis provides many physical insights to system dynamics. To this end, a first-order state variable implementation of the rotor inflow that can be efficiently linearized is a highly desirable feature for future advanced simulations. While state-space implementations of the free-vortex wake of a rotor exist, these implementations are complex and yield a very high number of states for typical flight dynamics simulations (*i.e.*, thousands or tens of thousands) (Refs. 1–6). When the rotor

Presented at the 50th European Rotorcraft Forum, Marseille, France, September 10–12, 2024.

speed is constant, these high-order aeromechanics models can be used to identify lower-order models or correction factors from frequency response data (Refs. 7, 8).

Another approach to model rotor-on-rotor interactions is to adopt low-order inflow models that are based on the Combined Momentum Theory and Simple Vortex Theory Inflow (CMTSVT) model (Refs. 9, 10). These models constitute the simplest inflow model for capturing the rotor-on-rotor inflow interference effects of generic multi-rotor configurations without requiring empirical tuning. These formulations of the inflow dynamics allow the interactional inflow dynamics to be time-marched yet still capture the flight dynamics of the multi-rotor aircraft. As such, multi-rotor aircraft simulations become self-contained and inherently linearizable, and thus do not require external processing to generate approximate linear models. Linearized models could then be used to assess the handling qualities of the vehicle, control law design, and for real-time simulations. A major challenge with the state-space free-wake implementation is making the resulting linearized models tractable for control design while still capturing the rotor-on-rotor interactional aerodynamics. In fact, the order of the linearized models will require being significantly reduced to remove the need for estimating or measuring the states associated with the rotor, inflow, and other high-order dynamics. Another challenge is the use of these reduced-order models that account for complex, and potentially adverse, aerodynamic interactions between rotors in model-following control architectures like dynamic inversion (DI) and explicit model following (EMF) to compensate aforementioned interactions, and to guarantee satisfactory stability, handling qualities, and performance requirements.

The objectives of the present investigation are articulated as follows: (i) implementation and linearization of low-order dynamic inflow models that account for the rotor-on-rotor interactional aerodynamics of coaxial compound helicopters; (ii) assessment the effect of the rotor-on-rotor interactional aerodynamics on the flight dynamics of a coaxial aircraft; and (iii) investigation of model-order reduction methods to guide the development of linearized models that are tractable for flight control design and predict the effect of rotor-on-rotor interactions on the vehicle flight dynamics. A coaxial aircraft is used in the simulation since flight dynamics impacts of the wake interactions are known (Ref. 11 and Chapter 7.4B in Ref. 12).

The paper begins with a detailed mathematical description of the dynamic modeling of rotor-on-rotor interactions, which follows that of Ref. 10. Next, the simulation model used in this study is presented. The model is trimmed and linearized in hover and cruise with rotor-on-rotor interactions enabled and disabled, and differences between the models are discussed. Model-order reduction methods are investigated to guide the development of linearized models that are tractable for flight control design while still predicting the effect of rotor-on-rotor interactions on the vehicle flight dynamics. Spectral- and frequency-response analyses are performed to assess any difference in stability and response characteristics between models with interactional aerodynamics accounted for and not. Results are qualitatively compared with flight-test data from previously published research studies. Final remarks summarize the study's overall findings and identify future developments.

ROTOR-ON-ROTOR INTERACTIONAL AERODYNAMICS

This section describes a recent extension (Ref. 13) of the state-space CMTSVT model (Refs. 9, 10) to rotors arbitrarily oriented in space and without necessarily the same radius and/or angular speed, as would be common in an eVTOL configuration. Consider the case where an arbitrary number N of rotors are sufficiently close such that their inflow dynamics is mutually interacting. For simplicity, consider two mutually-interacting rotors that are arbitrarily positioned and oriented in space and have radii that are not necessarily equal. This setup is shown in Fig. 1.

The inflow of the i^{th} rotor can be expressed as the summation between the self-induced inflow of that rotor and the interference inflow from all other rotors:

$$\boldsymbol{\lambda}_i = \boldsymbol{\lambda}_{\mathrm{s}_i} + \sum_{j=1, j\neq i}^{N} \boldsymbol{\lambda}_{\mathrm{int}_{ij}} \tag{1}$$

where:
$\boldsymbol{\lambda}_i^T = \begin{bmatrix}\lambda_{i_0} & \lambda_{i_{1c}} & \lambda_{i_{1s}}\end{bmatrix}$ is the total inflow of the i^{th} rotor in the local hub frame,
$\boldsymbol{\lambda}_{\mathrm{s}_i}^T = \begin{bmatrix}\lambda_{\mathrm{s}_{i_0}} & \lambda_{\mathrm{s}_{i_{1c}}} & \lambda_{\mathrm{s}_{i_{1s}}}\end{bmatrix}$ is the self-induced inflow of the i^{th} rotor in the local hub frame, and
$\boldsymbol{\lambda}_{\mathrm{int}_{ij}}^T = \begin{bmatrix}\lambda_{\mathrm{int}_{ij_0}} & \lambda_{\mathrm{int}_{ij_{1c}}} & \lambda_{\mathrm{int}_{ij_{1s}}}\end{bmatrix}$ is the interference inflow on the i^{th} from the j^{th} rotor in the i^{th} rotor hub frame.

The self-induced dynamics of the i^{th} rotor are given by:

$$\dot{\boldsymbol{\lambda}}_{\mathrm{s}_i} = \Omega \boldsymbol{T}_{W_i\to H_i} \boldsymbol{M}^{-1} \left[-\boldsymbol{L}_{ii}^{-1} \left(\boldsymbol{T}_{H_i\to W_i} \boldsymbol{\lambda}_{\mathrm{s}_i}\right) + \left(\boldsymbol{T}_{H_i\to W_i} \boldsymbol{F}_{ii}\right)\right] \tag{2}$$

where $\boldsymbol{M}$ is the apparent mass matrix, $\boldsymbol{L}$ is the composition of influence matrix, and where $\boldsymbol{T}_{W_i\to H_i}$ and $\boldsymbol{T}_{H_i\to W_i}$ are the transformation matrices from the rotor hub to the wind frame and vice versa. The apparent mass and composition of influence matrices are those from Pitt-Peters (Ref. 14) and are:

$$\boldsymbol{M} = \begin{bmatrix} \frac{8}{3\pi} & 0 & 0 \\ 0 & \frac{16}{45\pi} & 0 \\ 0 & 0 & \frac{16}{45\pi} \end{bmatrix} \tag{3}$$

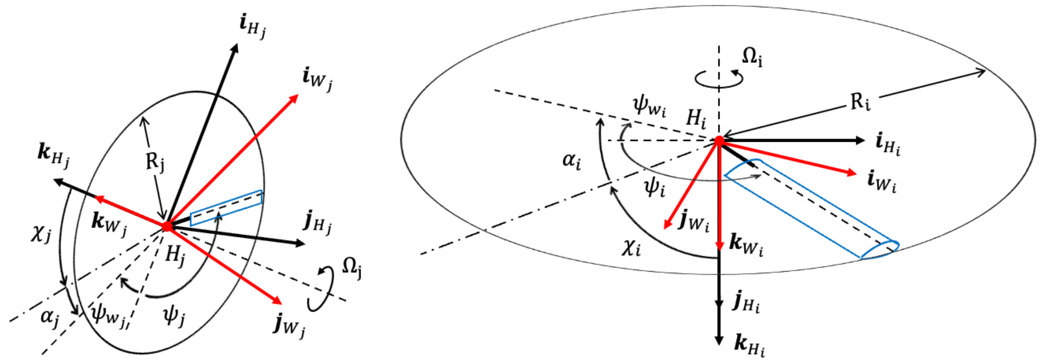

Fig. 1: Two mutually-interacting rotors that are arbitrarily positioned and oriented in space (Ref. 13).

$$\boldsymbol{L}_{ii} = \begin{bmatrix} \frac{0.5}{V_{T_i}} & -\frac{15\pi}{64V_i}\tan\frac{\chi_i}{2} & 0 \\ \frac{15\pi}{64V_{T_i}}\tan\frac{\chi_i}{2} & \frac{4\cos\chi_i}{V_i\,(1+\cos\chi_i)} & 0 \\ 0 & 0 & \frac{4}{V_i\,(1+\cos\chi)} \end{bmatrix} \tag{4}$$

Additionally, $\boldsymbol{F}_{ii}^T = [C_{T_i} \; -C_{M_i} \; -C_{L_i}]$, where C_{T_i}, C_{M_i}, and C_{L_i} are the aerodynamic thrust, pitching moment, and rolling moment coefficients of the i^{th} rotor in the local hub frame. The transformation from the i^{th} rotor hub frame to the i^{th} rotor wind frame is:

$$\begin{bmatrix} \boldsymbol{k}_{W_i} \\ \boldsymbol{j}_{W_i} \\ \boldsymbol{i}_{W_i} \end{bmatrix} = \underbrace{\begin{bmatrix} 1 & 0 & 0 \\ 0 & \cos\psi_{w_i} & -\sin\psi_{w_i} \\ 0 & \sin\psi_{w_i} & \cos\psi_{w_i} \end{bmatrix}}_{\boldsymbol{T}_{H_i\to W_i}} \begin{bmatrix} \boldsymbol{k}_{H_i} \\ \boldsymbol{j}_{H_i} \\ \boldsymbol{i}_{zh_i} \end{bmatrix} \tag{5}$$

where:

$$\psi_{w_i} = \begin{cases} \tan^{-1}\left(\frac{v_{H_i}}{u_{H_i}}\right), & \text{counterclockwise rotor} \\ \tan^{-1}\left(-\frac{v_{H_i}}{u_{H_i}}\right), & \text{clockwise rotor} \end{cases} \tag{6}$$

The total inflow and advance ratios of the i^{th} rotor are given by:

$$\mu_i = \frac{\sqrt{u_{H_i}^2 + v_{H_i}^2}}{\Omega_i R_i} \tag{7a}$$

$$\mu_{z_i} = \frac{w_{H_i}}{\Omega_i R_i} \tag{7b}$$

$$V_{T_i} = \sqrt{\mu_i^2 + \left(\mu_{z_i} - \lambda_{i_0}\right)^2} \tag{7c}$$

where u_{H_i}, v_{H_i}, and w_{H_i} are the longitudinal, lateral, and vertical velocity components of the i^{th} rotor hub. The skew angle of the i^{th} rotor is:

$$\chi_i = \tan^{-1}\left(\frac{\mu_i}{\lambda_{i_0} - \mu_{z_i}}\right) \tag{8}$$

The mass flow parameter is defined as:

$$V_i = \frac{\mu_i^2 + \left(\lambda_{i_0} - \mu_{z_i}\right)\left(2\lambda_{i_0} - \mu_{z_i}\right)}{V_{T_i}} \tag{9}$$

The interference inflow on the i^{th} from the j^{th} rotor is given by:

$$\boldsymbol{\lambda}_{\text{int}_{ij}} = \eta_{ij}\boldsymbol{L}_{ij}\boldsymbol{\lambda}_{\text{s}_j} \tag{10}$$

where η_{ij} is a parameter that scales the non-dimensional quantities of the j^{th} rotor to non-dimensional quantities of the i^{th} rotor:

$$\eta_{ij} = \frac{\Omega_j R_j}{\Omega_i R_i} \tag{11}$$

Note that this inflow scaling parameter generalizes CMTSVT to rotors with different radius and angular speed. The interference matrix $\boldsymbol{L}_{ij}$ is given by the multiplication of three matrices:

$$\boldsymbol{L}_{ij} = \boldsymbol{G}_{ij}\boldsymbol{R}_{\gamma_{ij}}\boldsymbol{L}_{jj} \tag{12}$$

where:

$$\boldsymbol{R}_{\gamma_{ij}} = \frac{1}{V_{T_j}\left(1 - 1.5\mu_j^2\right)} \begin{bmatrix} 1 & 0 & -3\mu_j \\ 0 & 3\left(1 - 1.5\mu_j^2\right) & 0 \\ -1.5\mu_j & 0 & 3 \end{bmatrix} \tag{13}$$

$$\boldsymbol{G}_{ij} = \begin{bmatrix} g_{00_{ij}} & g_{01s_{ij}} & g_{01c_{ij}} \\ g_{1s0_{ij}} & g_{1s1s_{ij}} & g_{1s1c_{ij}} \\ g_{1c0_{ij}} & g_{1c1s_{ij}} & g_{1c1c_{ij}} \end{bmatrix} \tag{14}$$

and where $\boldsymbol{L}_{jj}$ is the static inflow gain matrix defined above. The elements of the $\boldsymbol{G}_{ij}$ matrix are given by the following integrals:

$$g_{00_{ij}} = -\frac{1}{4\pi^2}\int_{-\psi_{w_i}}^{2\pi-\psi_{w_i}}\left[\int_0^{R_j/R_i}\left(\int_{-\psi_{w_j}}^{2\pi-\psi_{w_j}} K_{ij}d\psi_j\right)\hat{r}_i d\hat{r}_i\right]d\psi_i \tag{15a}$$

$$g_{01c_{ij}} = -\frac{1}{4\pi^2}\int_{-\psi_{w_i}}^{2\pi-\psi_{w_i}}\left[\int_0^{R_j/R_i}\left(\int_{-\psi_{w_j}}^{2\pi-\psi_{w_j}} K_{ij}\cos\psi_j d\psi_j\right)\hat{r}_i d\hat{r}_i\right]d\psi_i \tag{15b}$$

$$g_{01s_{ij}} = -\frac{1}{4\pi^2}\int_{-\psi_{w_i}}^{2\pi-\psi_{w_i}}\left[\int_0^{R_j/R_i}\left(\int_{-\psi_{w_j}}^{2\pi-\psi_{w_j}} K_{ij}\sin\psi_j d\psi_j\right)\hat{r}_i d\hat{r}_i\right]d\psi_i \tag{15c}$$

$$g_{1c0_{ij}} = -\frac{1}{\pi^2}\int_{-\psi_{w_i}}^{2\pi-\psi_{w_i}}\left[\int_0^{R_j/R_i}\left(\int_{-\psi_{w_j}}^{2\pi-\psi_{w_j}} K_{ij}d\psi_j\right)\hat{r}_i^2\cos\psi_i d\hat{r}_i\right]d\psi_i \tag{15d}$$

$$g_{1c1c_{ij}} = -\frac{1}{\pi^2}\int_{-\psi_{w_i}}^{2\pi-\psi_{w_i}}\left[\int_0^{R_j/R_i}\left(\int_{-\psi_{w_j}}^{2\pi-\psi_{w_j}} K_{ij}\cos\psi_j d\psi_j\right)\hat{r}_i^2\cos\psi_i d\hat{r}_i\right]d\psi_i \tag{15e}$$

$$g_{1c1s_{ij}} = -\frac{1}{\pi^2}\int_{-\psi_{w_i}}^{2\pi-\psi_{w_i}}\left[\int_0^{R_j/R_i}\left(\int_{-\psi_{w_j}}^{2\pi-\psi_{w_j}} K_{ij}\sin\psi_j d\psi_j\right)\hat{r}_i^2\cos\psi_i d\hat{r}_i\right]d\psi_i \tag{15f}$$

$$g_{1s0_{ij}} = -\frac{1}{\pi^2}\int_{-\psi_{w_i}}^{2\pi-\psi_{w_i}}\left[\int_0^{R_j/R_i}\left(\int_{-\psi_{w_j}}^{2\pi-\psi_{w_j}} K_{ij}d\psi_j\right)\hat{r}_i^2\sin\psi_i d\hat{r}_i\right]d\psi_i \tag{15g}$$

$$g_{1s1c_{ij}} = -\frac{1}{\pi^2}\int_{-\psi_{w_i}}^{2\pi-\psi_{w_i}}\left[\int_0^{R_j/R_i}\left(\int_{-\psi_{w_j}}^{2\pi-\psi_{w_j}} K_{ij}\cos\psi_j d\psi_j\right)\hat{r}_i^2\sin\psi_i d\hat{r}_i\right]d\psi_i \tag{15h}$$

$$g_{1s1s_{ij}} = -\frac{1}{\pi^2}\int_{-\psi_{w_i}}^{2\pi-\psi_{w_i}}\left[\int_0^{R_j/R_i}\left(\int_{-\psi_{w_j}}^{2\pi-\psi_{w_j}} K_{ij}\sin\psi_j d\psi_j\right)\hat{r}_i^2\sin\psi_i d\hat{r}_i\right]d\psi_i \tag{15i}$$

where j identifies the acting rotor whereas i represents the receiving rotor. To find the integrand function K_{ij}, one must first define the relative position of the rotors. Assume that the i^{th} rotor hub has the following (dimensional) coordinates expressed in the body frame:

$$\boldsymbol{r}_{\oplus\to H_i} = x_i\boldsymbol{i}_B + y_i\boldsymbol{j}_B + z_i\boldsymbol{k}_B \tag{16}$$

whereas the j^{th} rotor body-frame (dimensional) coordinates are:

$$\boldsymbol{r}_{\oplus\to H_j} = x_j\boldsymbol{i}_B + y_j\boldsymbol{j}_B + z_j\boldsymbol{k}_B \tag{17}$$

Then, the position of the i^{th} rotor with respect to the j^{th} rotor is:

$$\begin{aligned}\boldsymbol{r}_{H_j\to H_i} &= \boldsymbol{r}_{\oplus\to H_i} - \boldsymbol{r}_{\oplus\to H_j}\\ &= \boldsymbol{T}_{B\to H_j}\left(\begin{bmatrix}x_i\\ y_i\\ z_i\end{bmatrix} - \begin{bmatrix}x_j\\ y_j\\ z_j\end{bmatrix}\right)\\ &= x_{ij}\boldsymbol{i}_{H_j} + y_{ij}\boldsymbol{j}_{H_j} + z_{ij}\boldsymbol{k}_{H_j}\end{aligned} \tag{18}$$

The aerodynamic calculation points of the i^{th} rotor expressed in the j^{th} rotor hub coordinates are:

$$\begin{bmatrix}x_{\text{AC}_i}\\ y_{\text{AC}_i}\\ z_{\text{AC}_i}\end{bmatrix} = \begin{bmatrix}x_{ij}\\ y_{ij}\\ z_{ij}\end{bmatrix} + \underbrace{\boldsymbol{T}_{B\to H_j}\boldsymbol{T}_{H_i\to B}}_{\boldsymbol{T}_{H_i\to H_j}}\begin{bmatrix}-r_i\cos\psi_i\\ r_i\sin\psi_i\\ 0\end{bmatrix} \tag{19}$$

where r_i is the dimensional radial coordinate $0 \le r_i \le R_i$. The aerodynamic calculation points are non-dimensionalized with respect to the j^{th} rotor radius, such that:

$$\begin{bmatrix}\hat{x}_{\text{AC}_i}\\ \hat{y}_{\text{AC}_i}\\ \hat{z}_{\text{AC}_i}\end{bmatrix} = \frac{1}{R_j}\begin{bmatrix}x_{\text{AC}_i}\\ y_{\text{AC}_i}\\ z_{\text{AC}_i}\end{bmatrix} \tag{20}$$

Then, the interference of the j^{th} rotor on the i^{th} rotor can be computed according to Heyson (Ref. 15), such that:

$$J_{ij} = \frac{1-(-\hat{x}_{\text{AC}_i}\cos\psi_j + \hat{y}_{\text{AC}_i}\sin\psi_j) + R_c\sin\chi_j\cos\psi_j}{[R_c + (\cos\psi_j + \hat{x}_{\text{AC}_i})\sin\chi_j - \hat{z}_{\text{AC}_i}\cos\chi_j]R_c + r_c} \tag{21}$$

where:

$$\begin{aligned}R_c = \Big[1 &+ (-\hat{x}_{\text{AC}_i})^2 + \hat{y}_{\text{AC}_i}^2 + (-\hat{z}_{\text{AC}_i})^2\\ &- 2\left(-\hat{x}_{\text{AC}_i}\cos\psi_j + \hat{y}_{\text{AC}_i}\sin\psi_j\right)\Big]^{1/2}\end{aligned} \tag{22}$$

The variable r_c is the non-dimensional core radius of the tip vortex, which helps smooth out large induced velocities just to the right/left of the vortex tube (which are mathematically correct according to this formulation, but not necessarily physically accurate). A typical tip vortex core size value is approximately 5% of the rotor radius (Ref. 16). Thus, in this implementation, $r_c \approx 0.05$. Finally, the integrand function K_{ij} can be found as $K_{ij} = J_{ij}\left(\boldsymbol{k}_{H_j} \cdot \boldsymbol{k}_{H_i}\right)$ or, equivalently, $\boldsymbol{T}_{H_i \to H_{j_{3,3}}}$. It is worth noting that the total inflow harmonic coefficients $\boldsymbol{\lambda}_i$ are in fact an output of the system of dynamic inflow equations rather than states. Because these quantities are typically used to calculate the thrust coefficient and other variables before being computed in the inflow calculations, it is desirable to express them as states. This avoids algebraic loops in the rotor simulation and preserves the time-invariant formulation of the rotor dynamics. As such, the dynamics of the total inflow is expressed as a first-order filter with the following form:

$$\dot{\boldsymbol{\lambda}}_i = \frac{1}{\tau_\lambda}\left(\bar{\boldsymbol{\lambda}}_i - \boldsymbol{\lambda}_i\right) \tag{23}$$

where $\bar{\boldsymbol{\lambda}}_i$ is the total inflow calculated at each time step using Eq. (1), and τ_λ is the filter time constant which should be chosen as at least one order of magnitude faster than the fastest inflow dynamics. Based on this setup, the inflow dynamics has the following state vector:

$$\boldsymbol{x}_{\text{inflow}}^T = [\boldsymbol{\lambda}_{\text{s}_1} \cdots \boldsymbol{\lambda}_{\text{s}_N}\ \boldsymbol{\lambda}_1 \cdots \boldsymbol{\lambda}_N] \tag{24}$$

FLIGHT DYNAMICS SIMULATION MODEL

Configuration

This investigation makes use of the generic coaxial aircraft model based on Refs. 7 and 17 . This aircraft is shown qualitatively in Fig. 2 and its general characteristics are reported in Table 1. This configuration was chosen because experimental flight test data, which intrinsically captures the interference, exists from the flight test of the X2TD. Gross sizing and rotor geometry data of the aircraft come from the regression military model found in Ref. 18. Blade structural and mass properties were scaled using data from the Sikorsky XH-59 Advancing Blade Concept (Ref. 19) so that the first lag and flap modes match those of the advanced blade concept (ABC) technology demonstrator, roughly 1.3/rev for lag and 1.5/rev for flap. The same airfoils were used as in the XH-59 (Ref. 19).

Modeling

The software used for modeling the aircraft is HeliUM, a derivative of the one described in (Ref. 21). The rotorcraft flight dynamics are formulated as a nonlinear system of equations written in an implicit first-order form such that they are suitable for linearization, order reduction, and flight control design without any need for a constant mass matrix:

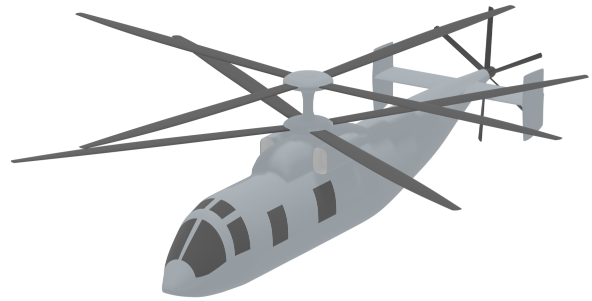

Fig. 2: Generic coaxial aircraft model (modified from original found in Ref. 7).

$$\mathbf{0} = \boldsymbol{f}(\dot{\boldsymbol{x}}, \boldsymbol{x}, \boldsymbol{u}, t) \tag{25a}$$

$$\boldsymbol{y} = \boldsymbol{g}(\dot{\boldsymbol{x}}, \boldsymbol{x}, \boldsymbol{u}, t) \tag{25b}$$

where $\boldsymbol{x} \in \mathbb{R}^n$ is the state vector, $\boldsymbol{u} \in \mathbb{R}^m$ is the control input vector, and $\boldsymbol{y} \in \mathbb{R}^l$ is the output vector. The state vector is:

$$\boldsymbol{x}^T = \left[\boldsymbol{x}_{\text{RB}}^T\ \boldsymbol{x}_{\text{R}_1}^T\ \boldsymbol{x}_{\text{R}_2}^T\right] \tag{26}$$

where $\boldsymbol{x}_{\text{RB}}$ are the rigid-body states and $\boldsymbol{x}_{\text{R}_i}$ are the states of the i^{th} rotor. The rigid-body (or fuselage) states are:

$$\boldsymbol{x}_{\text{RB}}^T = \left[u\ v\ w\ p\ q\ r\ \phi\ \theta\ \psi\right] \tag{27}$$

where:

$u,\ v,\ w$ are the longitudinal, lateral, and vertical velocities in the body-fixed frame,

$p,\ q,\ r$ are the roll, pitch, and yaw rates,

$\phi,\ \theta,\ \psi$ are the Euler angles, and

$x,\ y,\ z$ are the positions in the North-East-Down (NED) frame.

The state vector of the i^{th} rotor is:

$$\boldsymbol{x}_{\text{R}_i}^T = \left[\boldsymbol{\beta}_{\text{M}_i}^T\ \boldsymbol{\zeta}_{\text{M}_i}^T\ \boldsymbol{\lambda}_{\text{s}_i}^T\ \boldsymbol{\lambda}_i^T\right] \tag{28}$$

where:

$\boldsymbol{\beta}_{\text{M}_i}^T$ are finite-element displacement and derivative states corresponding to a blade structural mode that is predominantly flapping,

$\boldsymbol{\zeta}_{\text{M}_i}^T$ are finite-element states corresponding to a blade mode that has predominantly lead-lag motion, and

$\boldsymbol{\lambda}_{\text{s}_i}$ and $\boldsymbol{\lambda}_i$ are the self-induced and total inflow velocities of the i^{th} rotor.

The pilot input vector is:

$$\boldsymbol{u}^T = \left[\delta_{\text{lat}}\ \delta_{\text{lon}}\ \delta_{\text{col}}\ \delta_{\text{ped}}\ \delta_{\text{aux}}\right] \tag{29}$$

where:

δ_{lat} is the lateral stick position,

δ_{lon} are the lateral and longitudinal stick positions,

Table 1: General characteristics of the generic coax model (Ref. 20).

Parameter	**Value**	**Units**
Mass and inertia		
Gross weight, W	35185	lb
Roll-axis moment of inertia, I_{xx}	10235	sl-ft^2
Pitch-axis moment of inertia, I_{yy}	84610	sl-ft^2
Yaw-axis moment of inertia, I_{zz}	80840	sl-ft^2
Roll/yaw-axes product of inertia, I_{xz}	0	sl-ft^2
Fuselage		
Drag Area	8.7	ft^2
CG Longitudinal Location (body axes)	-1.5	ft
CG Lateral Location (body axes)	0	ft
CG Vertical Location (body axes)	0.42	ft
Rotors		
Number of blades	4	-
Radius	30.55	ft
Blade max chord	3.23	ft
Blade twist	-9	deg
Blade weight	1133	lbs
Rotational Speed (Hover)	23.7	rad/s
Rotational Speed (Cruise)	19.0	rad/s
Rotor Vertical Separation	4.275	ft
Longitudinal Location (body axes)	0	ft
Lateral Location (body axes)	0	ft
Vertical Location (body axes)	$\{-4.67, -8.94\}$	ft
Pusher Propeller		
Number of blades	6	-
Radius	6.6	ft
Blade chord	0.62	ft
Blade twist	-40	deg
Rotational Speed (Hover)	136	rad/s
Rotational Speed (Cruise)	109	rad/s
Longitudinal Location (body axes)	-31.83	ft
Lateral Location (body axes)	0	ft
Vertical Location (body axes)	2.00	ft
Horizontal Stabilizer		
Span	20	ft
Chord	6	ft
Longitudinal Location (body axes)	-25.83	ft
Lateral Location (body axes)	0	ft
Vertical Location (body axes)	3.00	ft
Vertical Stabilizers (Center)		
Surface Area	10	ft^2
Longitudinal Location (body axes)	-25.83	ft
Lateral Location (body axes)	0	ft
Vertical Location (body axes)	0	ft
Vertical Stabilizers (Side)		
Surface Area	20	ft^2
Longitudinal Location (body axes)	-25.83	ft
Lateral Location (body axes)	$\{10, -10\}$	ft
Vertical Location (body axes)	0	ft

δ_{col} is the collective stick position,
δ_{ped} is the pedal position, and
δ_{aux} is an auxiliary input that controls the pusher propeller collective pitch angle.

Linearization and Model-Order Reduction

Upon trimming the aircraft dynamics at a desired flight condition, the coupled rigid-body and rotor dynamics can be linearized about that trim solution using perturbation methods (Refs. 5, 22) to yield a linear time-invariant (LTI) system in first-order form. The state vector is passed through a multi-blade coordinate transformation to convert individual blade states to multi-blade coordinates:

$$\dot{\boldsymbol{x}} = \boldsymbol{A}\boldsymbol{x} + \boldsymbol{B}\boldsymbol{u} \tag{30a}$$

$$\boldsymbol{y} = \boldsymbol{C}\boldsymbol{x} + \boldsymbol{D}\boldsymbol{u} \tag{30b}$$

where $\boldsymbol{A} \in \mathbb{R}^{n\times n}$ is the system matrix, $\boldsymbol{B} \in \mathbb{R}^{n\times m}$ is the control matrix, $\boldsymbol{C} \in \mathbb{R}^{l\times n}$ is the output matrix, and $\boldsymbol{D} \in \mathbb{R}^{l\times m}$ is the feed-through matrix. It is desirable to reduce the order of the linearized dynamics to: (i) be able to extract the stability and control derivatives of the rigid-body dynamics, and (ii) make the linearized models tractable for control design; both while still capturing the rotor-on-rotor interactional aerodynamics. Because the rotor (*i.e.*, inflow, flapping, and lead-lag) dynamics are typically stable and significantly faster than that of the rigid-body dynamics, the order of the coupled rigid-body and rotor dynamics can be reduced by means of singular perturbation theory, and in particular via residualization (Ref. 23). This approach removes the need to measure or estimate higher-order dynamics states associated with the rotors and their inflow dynamics while retaining information on the influence of the residualized dynamics onto the slower rigid-body dynamics (Ref. 24).

Assuming one or more states to have stable dynamics which are faster than that of the remaining states, the state vector in Eq. (26) is partitioned into slow and fast components:

$$\boldsymbol{x}^T = \begin{bmatrix}\boldsymbol{x}_{\text{s}}^T \ \boldsymbol{x}_{\text{f}}^T\end{bmatrix} \tag{31}$$

Then, the system in Eq. (30a) can be re-written as:

$$\begin{bmatrix}\dot{\boldsymbol{x}}_{\text{s}} \\ \dot{\boldsymbol{x}}_{\text{f}}\end{bmatrix} = \begin{bmatrix}\boldsymbol{A}_{\text{s}} & \boldsymbol{A}_{\text{sf}} \\ \boldsymbol{A}_{\text{fs}} & \boldsymbol{A}_{\text{f}}\end{bmatrix}\begin{bmatrix}\boldsymbol{x}_{\text{s}} \\ \boldsymbol{x}_{\text{f}}\end{bmatrix} + \begin{bmatrix}\boldsymbol{B}_{\text{s}} \\ \boldsymbol{B}_{\text{f}}\end{bmatrix}\boldsymbol{u} \tag{32}$$

By neglecting the dynamics of the fast states (*i.e.*, $\dot{\boldsymbol{x}}_{\text{f}} = 0$) and performing a few algebraic manipulations, the equations for a reduced-order system with the state vector composed of the slow states may be found:

$$\dot{\boldsymbol{x}}_{\text{s}} = \hat{\boldsymbol{A}}\boldsymbol{x}_{\text{s}} + \hat{\boldsymbol{B}}\boldsymbol{u} \tag{33}$$

where:

$$\hat{\boldsymbol{A}} = \boldsymbol{A}_{\text{s}} - \boldsymbol{A}_{\text{sf}}\boldsymbol{A}_{\text{f}}^{-1}\boldsymbol{A}_{\text{fs}} \tag{34a}$$

$$\hat{\boldsymbol{B}} = \boldsymbol{B}_{\text{s}} - \boldsymbol{A}_{\text{sf}}\boldsymbol{A}_{\text{f}}^{-1}\boldsymbol{B}_{\text{f}} \tag{34b}$$

Note that $\boldsymbol{A}_{\text{f}}$ must be invertible. This is guaranteed if $\boldsymbol{A}_{\text{f}}$ is asymptotically stable, *i.e.*, all eigenvalues have their real part that is strictly negative. This condition is satisfied by choosing the rotor dynamics as the fast dynamics, since the rotor dynamics are typically stable with eigenvalues on the far left of the complex plane. Consequently, the slow states are chosen as the rigid-body states with the exception of the position and heading states which are truncated as the rotorcraft dynamics are invariant with respect to these states (Ref. 25):

$$\boldsymbol{x}_{\text{s}} = \boldsymbol{x}_{\text{RB}} \tag{35a}$$

$$\boldsymbol{x}_{\text{f}}^T = \begin{bmatrix}\boldsymbol{x}_{\text{R}_1}^T \ \boldsymbol{x}_{\text{R}_2}^T\end{bmatrix} \tag{35b}$$

This way, an 8-state residualized system is obtained that still accounts for the higher-order dynamics. For the model to retain information about the influence of the residualized dynamics on the outputs, consider partitioning the output equations in Eq. (30b) as:

$$\boldsymbol{y} = \begin{bmatrix}\boldsymbol{C}_{\text{s}} & \boldsymbol{C}_{\text{f}}\end{bmatrix}\begin{bmatrix}\boldsymbol{x}_{\text{s}} \\ \boldsymbol{x}_{\text{f}}\end{bmatrix} + \boldsymbol{D}\boldsymbol{u} \tag{36}$$

Then, it can be shown that the residualized output equations are:

$$\dot{\boldsymbol{Y}} = \hat{\boldsymbol{C}}\boldsymbol{x}_{\text{s}} + \hat{\boldsymbol{D}}\boldsymbol{u} \tag{37}$$

where:

$$\hat{\boldsymbol{C}} = \boldsymbol{C}_{\text{s}} - \boldsymbol{C}_{\text{f}}\boldsymbol{A}_{\text{f}}^{-1}\boldsymbol{A}_{\text{fs}} \tag{38a}$$

$$\hat{\boldsymbol{D}} = \boldsymbol{D} - \boldsymbol{C}_{\text{f}}\boldsymbol{A}_{\text{f}}^{-1}\boldsymbol{B}_{\text{f}} \tag{38b}$$

These residualized models are used for capturing the influence of rotor-on-rotor interactions on the stability and control derivatives.

RESULTS

Trim

The generalized CMTSVT model is implemented within HeliUM for the Generic Coax configuration. Examples of interference matrices (*i.e.*, the matrix $\boldsymbol{G}$) computed based on the generic coax geometry, shown in Fig. 3, are provided below:

$$\boldsymbol{G}_{12} = \begin{bmatrix}0.3595 & 0 & 0 \\ 0 & 0.0841 & 0 \\ 0 & 0 & 0.0851\end{bmatrix} \tag{39a}$$

$$\boldsymbol{G}_{21} = \begin{bmatrix}0.5741 & 0 & 0 \\ 0 & 0.3021 & 0 \\ 0 & 0 & 0.3054\end{bmatrix} \tag{39b}$$

(39c)

The matrix $\boldsymbol{G}_{12}$ represents the interference of rotor 2 (lower) on rotor 1 (upper), whereas the opposite is true for

$\boldsymbol{G}_{21}$. As expected, the influence of rotor 2 on rotor 1 is of a lesser entity given that rotor 2 acts in the wake of rotor 1. Because rotors 1 and 2 are coaxial, only on-axis terms are non-zero in the $\boldsymbol{G}_{12}$ and $\boldsymbol{G}_{21}$ matrices.

Next, the simulation is trimmed at hover to find the steady-state self-induced and total inflow ratio values, as well as the rotors' thrust and power. These values are reported in Table 2 and show that while the self-induced inflow is higher for the upper rotor, the total inflow is higher for the lower rotor. This is explained by the fact that the lower rotor acts in the wake of the upper rotor, such that it effectively operates in an axial climb. The equivalent axial climb velocity (*i.e.*, the downwash from the upper rotor) reduces the self-induced inflow – compared to hover values for the isolated rotor – while increasing the total inflow through that rotor. Because the self-induced inflow of the upper rotor is higher than the lower rotor, the thrust produced by the upper rotor is also higher. On the other hand, no significant changes in power are observed. To quantify the effect of rotor-on-rotor interactions on power compared to the case of two isolated rotors, consider computing the interference-induced power factor (Ref. 26):

$$k_{\text{int}} = 2\sqrt{2}\left(\frac{T_{\text{u}}}{T_{\text{l}}}\right)^{3/2}\left(1+\frac{T_{\text{u}}}{T_{\text{l}}}\right)^{-3/2} = 1.172 \qquad (40)$$

where T_{u} and T_{l} are the thrusts of the upper and lower rotor, respectively. This value is similar to that reported in Ref. 26, *i.e.*, $k_{\text{int}} = 1.266$ for coaxial rotors operated at equal rotor torque and with the lower rotor operating in the far wake of the upper rotor. Differences in these results may be attributed to the fact that, in reality, the lower rotor does not fully act in the wake of the upper rotor, but rather, the upper rotor wake only affects a portion of the lower rotor. However, the CMTSVT model adopted herein does not model wake decay and/or contraction. Wake decay and contraction effects could possibly be implemented based on Ref. 27.

Bare-Airframe Dynamics

Next, the model is linearized about the hover trim condition and subsequently residualized to assess the effect of the interactional dynamics on the rigid-body dynamics. Figure 4 shows the eigenvalues of the residualized dynamics with and without rotor-on-rotor interactions. The latter case is achieved by conveniently setting the interference matrices G to zero. Numerical values for the eigenvalues, as well as the modal properties of the corresponding modes, are reported quantitatively in Table 3. These results show that rotor-on-rotor interactions have some effect on the hovering cubic (Ref. 28) eigenvalues. More specifically, roll and pitch oscillation modes result in higher natural frequencies whereas the frequencies of the roll and pitch subsidence modes are seen to decrease. On the other hand, the vertical (heave) and directional (yaw) dynamics appear to be largely unaffected. It is concluded that, for this particular coaxial configuration, the rotor-on-rotor interactional aerodynamics impacts only the lateral and longitudinal axes.

Table 2: Performance of the counter-rotating coaxial rotors trimmed at hover.

Variable	Units	Rotor 1 (Upper)	Rotor 2 (Lower)
λ_0	-	0.062	0.076
λ_{1c}	-	0.005	0006
λ_{1s}	-	-0.000	-0.000
λ_{S_0}	-	0.042	0.028
$\lambda_{S_{1c}}$	-	0.004	0.002
$\lambda_{S_{1s}}$	-	-0.000	-0.000
T	lb	19298	15425
C_T	-	0.0053	0.0042
P	hp	2098	2098
C_P	-	0.00044	0.00044

To better explain these differences, the stability derivatives of the residualized dynamics are investigated. Consider the decoupled, reduced-order, lateral dynamics:

$$\begin{bmatrix}\dot{v}\\ \dot{p}\\ \dot{\phi}\end{bmatrix} = \begin{bmatrix}Y_v & 0 & g\\ L_v & L_p & 0\\ 0 & 1 & 0\end{bmatrix}\begin{bmatrix}v\\ p\\ \phi\end{bmatrix} + \begin{bmatrix}0\\ L_{\delta_{\text{lat}}}\\ 0\end{bmatrix}\delta_{\text{lat}} \qquad (41)$$

Note that, at hover and for a symmetric configuration like the generic coax configuration, the lateral dynamics is decoupled from the directional dynamics. The stability and control derivatives corresponding to the lateral dynamics are reported in Table 4. Rotor-on-rotor interactions result in a roll rate response due to lateral velocity (*i.e.*, L_v) that is lower in magnitude and in a roll damping (*i.e.*, L_p) that is also significantly lower in magnitude. The lower magnitude of L_p explains the lower frequency of the roll subsidence mode when compared to the case of no rotor-on-rotor interactions, whereas the combination of L_v and L_p results in a higher-frequency roll oscillation mode.

Now consider the decoupled, reduced-order, longitudinal dynamics system matrix:

$$\begin{bmatrix}\dot{u}\\ \dot{q}\\ \dot{\theta}\end{bmatrix} = \begin{bmatrix}X_u & 0 & -g\\ M_u & M_q & 0\\ 0 & 1 & 0\end{bmatrix}\begin{bmatrix}u\\ q\\ \theta\end{bmatrix} + \begin{bmatrix}0\\ M_{\delta_{\text{lon}}}\\ 0\end{bmatrix}\delta_{\text{lon}} \qquad (42)$$

For a symmetric configuration like the generic coax, the longitudinal dynamics and vertical dynamics are also decoupled at hover. The stability and control derivatives corresponding to the longitudinal dynamics are reported in Table 5. Similarly to the case of the lateral dynamics, rotor-on-rotor interactions result in a pitch rate response due

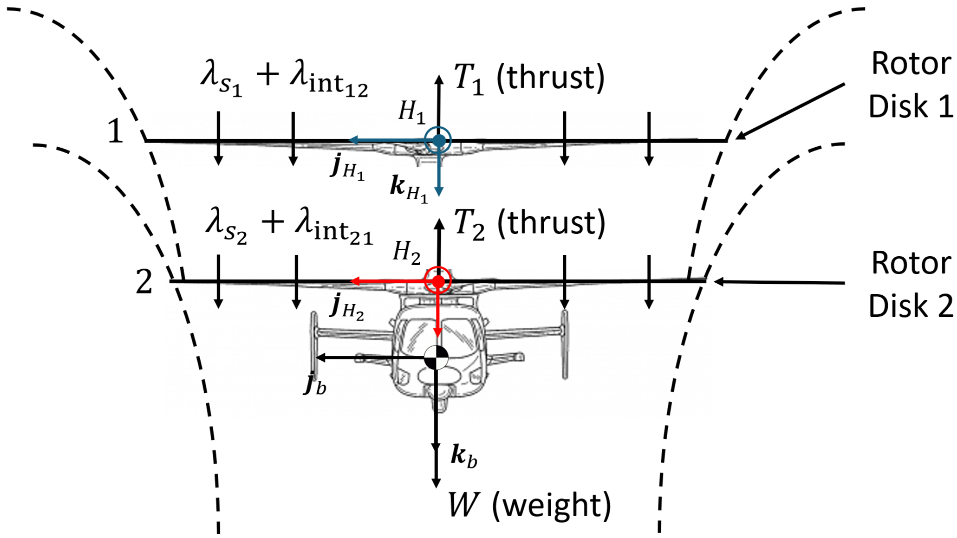

Fig. 3: Rotor numbering convention.

Table 3: Hover modal characteristics with and without rotor-on-rotor interactions.

Mode	Interactional Aerodynamics	Eigenvalues [rad/s]	Natural Frequency, ω_n [rad/s]	Damping Ratio, ζ
Roll Subsidence	Off	-8.368	-	1
	On	-5.384	-	1
Pitch Subsidence	Off	-3.880	-	1
	On	-3.444	-	1
Roll Oscillation	Off	$0.032 \pm 0.759i$	0.760	-
	On	$0.077 \pm 0.847i$	0.850	-
Pitch Oscillation	Off	$0.042 \pm 0.608i$	0.609	-
	On	$0.052 \pm 0.682i$	0.684	-
Heave Subsidence	Off	-0.398	-	1
	On	-0.315	-	1
Yaw Subsidence	Off	-0.061	-	1
	On	-0.111	-	1

to longitudinal velocity (*i.e.*, M_u) that is lower in magnitude and in a pitch damping (*i.e.*, M_q) that is also significantly lower in magnitude. The lower magnitude of M_q explains the lower frequency of the pitch subsidence mode when compared to the case of no rotor-on-rotor interactions, whereas the combination of M_u and M_q results in a higher-frequency pitch oscillation mode. It is concluded that rotor-on-rotor interactions result in a lower magnitude roll/pitch rate response to lateral/longitudinal velocity and in a lower pitch/roll damping. In turn, the combination of these effects yields roll and pitch subsidence modes at a lower frequency, and roll and pitch oscillation modes with a higher natural frequency.

To further explain the effect of rotor-on-rotor interactions on the hover flight dynamics, on-axis frequency responses are computed based on the full-order dynamics with and without interactional aerodynamics. Figure 5 shows the roll and pitch on-axis frequency responses with and without rotor-on-rotor interactions. The roll-axis frequency responses including interference show higher magnitude and lower phase at low to medium frequencies (*i.e.*, approximately 0.7 to 10 rad/s), which is consistent with results from the Sikorsky X2TD flight test. In an initial validation of the HeliUM model against the X2TD flight test data, there were no interference effects and there was a similar underprediction of the response (Ref. 8). On the other hand, the CMTSVT based pitch-axis response shows very similar magnitude and phase at the same frequencies, while some

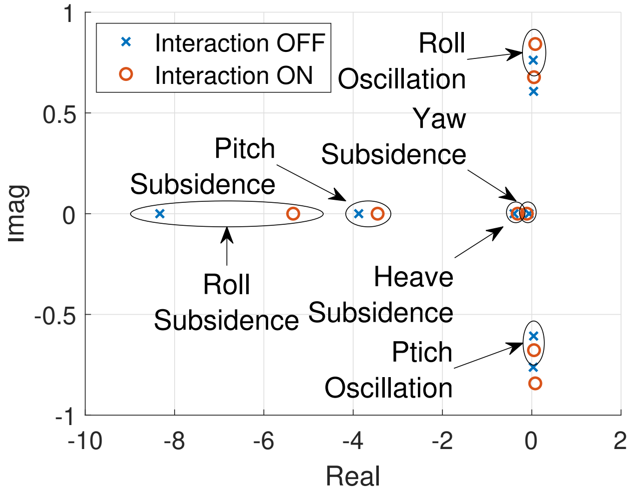

Fig. 4: Comparison between the residualized dynamics eigenvalues at hover with and without rotor-on-rotor interactions.

Table 4: Lateral stability and control derivatives.

Parameter	Interactional Aerodynamics	Value	Units
Y_v	Off	0.115	1/s
	On	0.082	
L_v	Off	-0.148	rad/(ft-s)
	On	-0.111	
L_p	Off	-8.433	1/s
	On	-5.378	
$L_{\delta_{\text{lat}}}$	Off	2.124	rad/(s^2-%)
	On	2.066	

Table 5: Longitudinal stability and control derivatives.

Parameter	Interactional Aerodynamics	Value	Units
X_u	Off	0.0085	1/s
	On	0.0091	
M_u	Off	0.045	rad/(ft-s)
	On	0.054	
M_q	Off	-3.782	1/s
	On	-3.277	
$M_{\delta_{\text{lon}}}$	Off	0.663	rad/(s^2-%)
	On	0.642	

differences are apparent at lower frequencies (*i.e.*, less than 0.7 rad/s). This is also consistent with the X2TD model validation, where neglecting interference effects didn't impact the pitch axis significantly.

With the interference effects turned on, the responses have similar trends to that of the flight test data of the X2TD when compared to no interference effects. Though a different aircraft, the trends are expected to be the same, giving confidence in the CMTSVT model's ability to correctly capture the dynamic response.

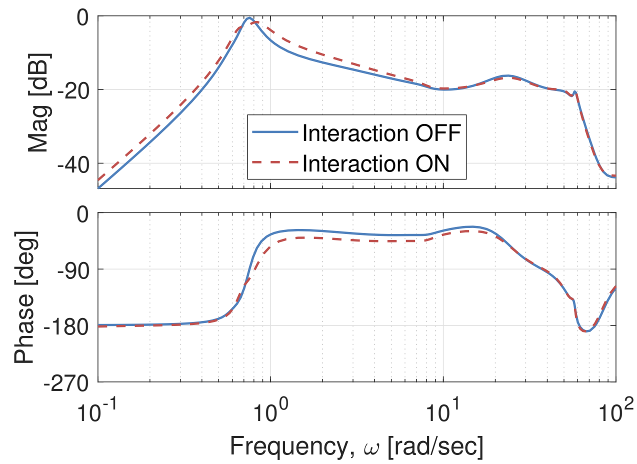

(a) $\frac{p}{\delta_{\text{lat}}}(s)$

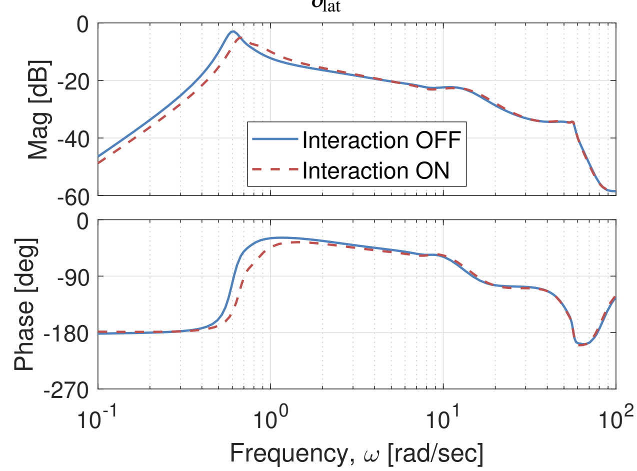

(b) $\frac{q}{\delta_{\text{lon}}}(s)$

Fig. 5: Roll and pitch on-axis frequency responses with and without rotor-on-rotor interactions in hover

Figure 6 shows the directional and heave on-axis frequency responses with and without rotor-on-rotor interactions. The directional axis response (Fig. 6a) shows a higher magnitude in the low to medium frequency range for the case of rotor-on-rotor interactions while the phase is approximately the same. On the other hand, no significant change in magnitude or phase is seen for the vertical axis response (Fig. 6b). These results further substantiate the observations based on the spectral and modal analyses.

On-axis frequency responses are also computed for the case of forward flight at 80 kts. As shown in Fig. 7a, differences between rotor-on-rotor interactions on are only apparent at low frequencies. Similar observations can be made for

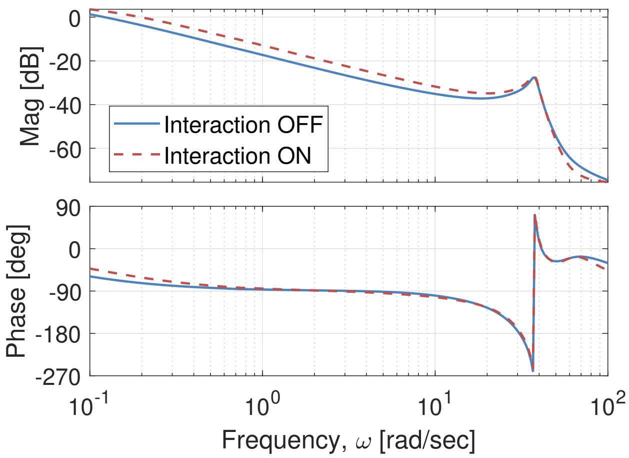

(a) $\frac{r}{\delta_{\text{ped}}}(s)$

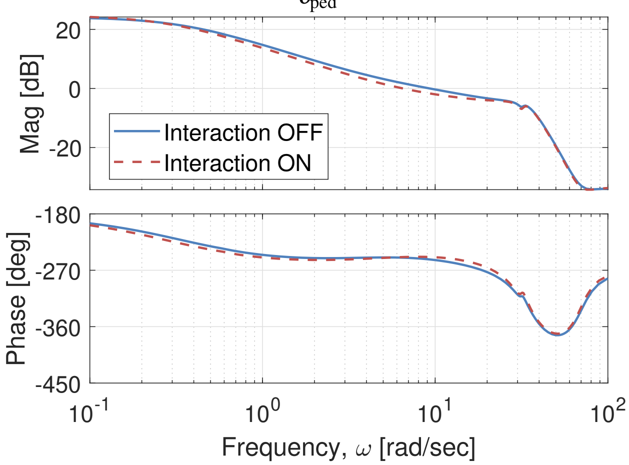

(b) $\frac{w}{\delta_{\text{col}}}(s)$

Fig. 6: Yaw and Heave on-axis frequency responses with and without rotor-on-rotor interactions in hover

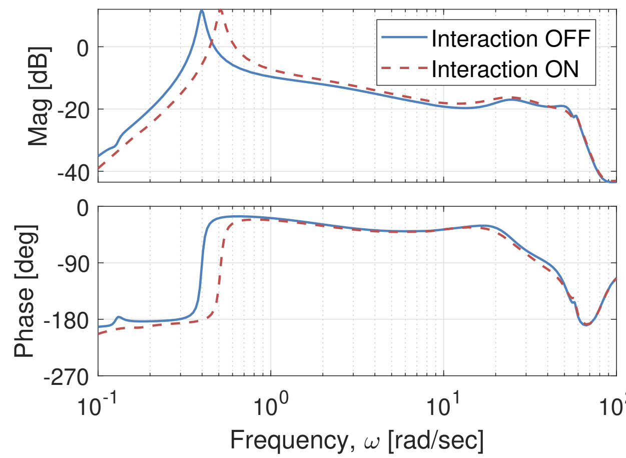

(a) $\frac{p}{\delta_{\text{lat}}}(s)$

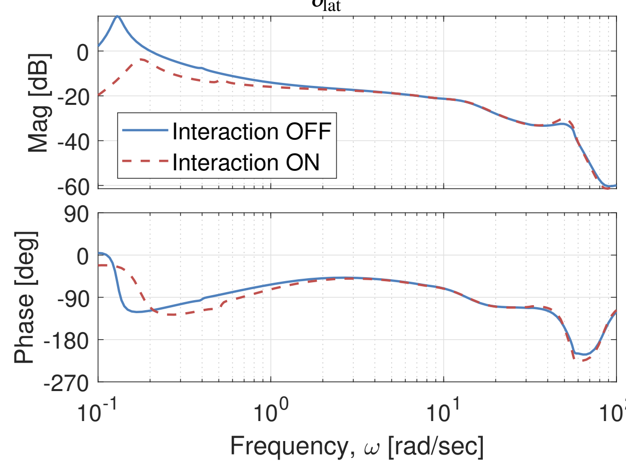

(b) $\frac{q}{\delta_{\text{lon}}}(s)$

Fig. 7: Roll and pitch on-axis frequency responses with and without rotor-on-rotor interactions at 80 knots

longitudinal- and directional-axis responses, shown in Fig. 7b. The vertical axis frequency responses, shown in Fig. 8b do not show particular differences between rotor-on-rotor interactions on and off. As with the hover results, these observations are all consistent with X2TD data in Ref. 8. In that work, there is little effect of interference in the roll axis, but the pitch axis showed a marked decrease in magnitude at low frequency, the same trends are seen here.

SUMMARY AND CONCLUSIONS

This paper focused on the integration of a generalized rotor-on-rotor interactional aerodynamics model in state-variable form within a flight dynamics simulation and on its subsequent linearization and linear model analysis. The aircraft chosen for this investigation is a generic lift-offset compound coaxial rotorcraft. Upon trimming the flight dynamics at hover, linearized models of the dynamics were compared to nonlinear simulations, and with baseline models that do not account for rotor-on-rotor inflow interference effects. Model-order reduction methods were investigated to guide the development of linearized models that are tractable for flight control design while still predicting the effect of rotor-on-rotor interactions on the vehicle flight dynamics. Linear model analysis was performed to assess any difference in stability and response characteristics between models with interactional aerodynamics accounted for and not. Results were compared with flight-test data from previously published research studies. Based on this work, the following conclusions can be reached:

1. The CMTSVT model, as implemented in the HeliUM flight dynamics code, correctly captures trim impacts from the interacting wakes. This is validated against momentum theory based coaxial rotor performance models.

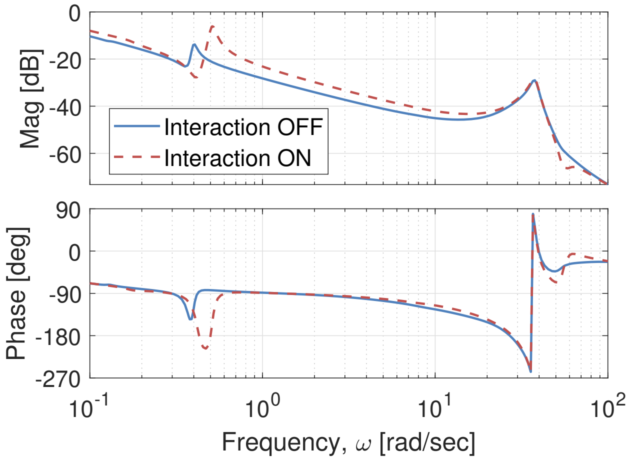

(a) $\frac{r}{\delta_{\text{ped}}}(s)$

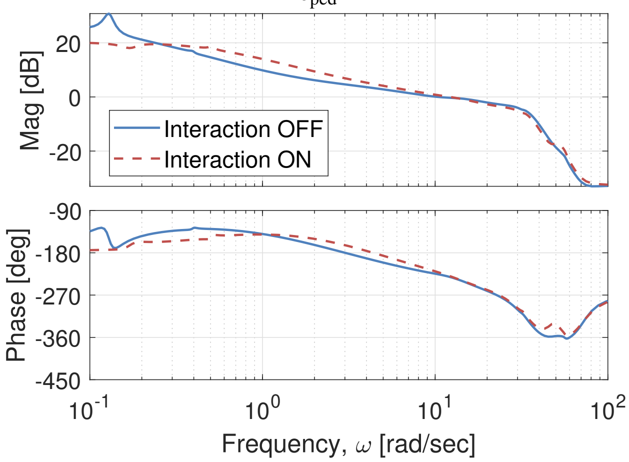

(b) $\frac{w}{\delta_{\text{col}}}(s)$

Fig. 8: Vertical axis frequency responses with and without rotor-on-rotor interactions at 80 knots

2. For the coaxial configuration in hover, the rotor-on-rotor interactional aerodynamics results in small changes in the frequencies of the roll and pitch oscillatory modes. The largest impact of the interference is on the magnitude and phase of the roll response between 0.7 and 10 rad/sec, where the response has an elevated magnitude and decreased phase.

3. The hover impacts of the interactional aerodynamics show the same trends as those observed in flight test data of the Sikorsky X2TD.

4. In forward flight, the interactional aerodynamics impacts the pitch response in the same way as flight test data from the Sikorsky X2TD. The interference reduces the low frequency response magnitude in this axis.

Future work will focus on a thorough validation of CMTSVT against other dynamic inflow models for coaxial rotors found in the literature, as well as assessing any impact of rotor-on-rotor interactions on flight control design.

ACKNOWLEDGMENTS

This work was funded in part by the US Army Combat Capabilities Development Command (DEVCOM) Aviation & Missile Center (AvMC) under the Joint Tactical Aerial Resupply Vehicle (JTARV) project with Dr. Mark Lopez as the technical monitor and Ms. Emily Glover as the POC under agreement no. 2116146093UMD. This work was also funded in part by the Vertical Lift Research Center of Excellence (VLRCOE) with Dr. Mahendra Bagwhat as the technical monitor and Mr. Eric Tobias as the Technical POC. The authors would like to thank DEVCOM AvMC for their project support, guidance, discussions, and feedback.

REFERENCES

[1]Celi, R., "State-Space Representation of Vortex Wakes by the Method of Lines," *Journal of the American Helicopter Society*, Vol. 50, (2), Apr 2005, pp. 195–205.
doi: https://doi.org/10.4050/1.3092855

[2]Saetti, U. and Horn, J. F., "Implementation and Linearization of a Rotor Simulation with a State-Space Free-Vortex Wake Model," Proceedings of the 78th Annual Forum of the Vertical Flight Society, May 10-12, 2022.
doi: https://doi.org/10.4050/F-0078-2022-17577

[3]Saetti, U., "Linearization of a Rotor Simulation with a State-Space Free-Vortex Wake Model in a Shipboard Environment," Proceedings of the AIAA Aviation Forum, Chicago, IL & Virtual, Jun 27 - Jul 1, 2022.
doi: https://doi.org/10.2514/6.2022-3646

[4]Saetti, U. and Horn, J. F., "Implementation and Linearization of State-Space Free-Vortex Wake Models for Rotary- and Flapping-Wing Vehicles," *Journal of the American Helicopter Society*, Vol. 68, (4), Apr 2023, pp. 42004–42017.
doi: https://doi.org/10.4050/JAHS.68.042004

[5]Saetti, U. and Horn, J. F., "Tiltrotor Simulations with Coupled Flight Dynamics, State-Space Aeromechanics, and Aeroacoustics," *Journal of the American Helicopter Society*, Vol. 69, (1), Apr 2024.
doi: https://doi.org/10.4050/JAHS.69.012003

[6]Hafez, H., Cocco, A., and Saetti, U., "Implementation, Linearization, and Order Reduction of a Coupled Panel and Free-Wake Method in State-Space Form," Proceedings of the AIAA SciTech Forum, Jan 8-12, 2024.
doi: https://doi.org/10.2514/6.2024-2265

[7]Hersey, S., Celi, R., Tischler, M. B., Juhasz, O., Rand, O., and Khromov, V., "State-Space Inflow Model Identification and Flight Dynamics Coupling for an Advanced Coaxial Rotorcraft Configuration," Proceedings of the 73rd Annual Forum of the Vertical Flight Society, May 9-11, 2017.

[8]Fegely, C. E., Xin, H., Tischler, M., and Juhasz, O., "Flight Dynamics and Control Modeling with System Identification Validation of the Sikorsky X2 Technology Demonstrator," Proceedings of the 72$^{\text{nd}}$ Annual Forum of the American Helicopter Society, 05 2016.

[9]Guner, F. and Prasad, J. V. R., "Combined Momentum Theory and Simple Vortex Theory Inflow Model for Multirotor Configurations," *Journal of the American Helicopter Society*, Vol. 67, (2), jan 2022, pp. 1–15.
doi: https://doi.org/10.4050/JAHS.67.022007

[10]Guner, F., "A Multirotor Inflow Model Based on Combined Momentum Theory and Simple Vortex Theory (CMTSVT) for Flight Simulations," Proceedings of the 78$^{\text{th}}$ Forum of the Vertical Flight Society, May 10-12, 2022.
doi: https://doi.org/10.4050/F-0078-2022-17579

[11]Keller, J., McKillip, R., Wachspress, D., Tischler, M., and Juhasz, O., "Linearized Inflow and Interference Models from High Fidelity Free Wake Analysis for Modern Rotorcraft Configurations," Proceedings of the 75th Annual Forum of the Vertical Flight Society, May 14-15, 2019.
doi: https://doi.org/10.4050/F-0075-2019-14638

[12]Tischler, M. B., White, M., *et al.*, "Rotorcraft Flight Simulation Model Fidelity Improvement and Assessment," Technical Report AVT-296, NATO, Dec 2020.

[13]Saetti, U. and Guner, F., "Interactional Aerodynamics Modeling and Flight Control Design of Multi-Rotor Aircraft," Proceedings of the 6$^{\text{th}}$ Decennial Aeromechanics Specialits' Conference, Santa Clara, CA, Feb 6–8, 2024.

[14]Pitt, D. M. and Peters, D. A., "Theoretical Prediction of Dynamic-Inflow Derivatives," Proceedings of the 6$^{\text{th}}$ European Rotorcraft and Powered Lift Aircraft Forum, September 16-19, 1980.

[15]Heyson, H. H., "Equations for the Induced Velocities Near a Lifting Rotor with Nonuniform Azimuthwise Vorticity Distribution," Technical report, NASA TN D394, August 1960.

[16]Bhagwat, M. J. and Leishman, J. G., "Correlation of Helicopter Rotor Tip Vortex Measurements," *AIAA Journal*, Vol. 38, (2), 2000, pp. 301–308.
doi: https://doi.org/10.2514/2.957

[17]Berger, T., Juhasz, O., Lopez, M. J. S., Tischler, M. B., and Horn, J. F., "Modeling and Control of Lift Offset Coaxial and Tiltrotor Rotorcraft," *CEAS Aeronautical Journal*, August 2019.
doi: 10.1007/s13272-019-00414-0

[18]Johnson, W., Moodie, A., and Yeo, H., "Design and Performance of Lift-Offset Rotorcraft for Short-Haul Missions," AHS Future Vertical Lift Aircraft Design Conference, San Francisco, CA, Jan 18-20, 2012.

[19]Ruddell, A. J., "XH-59A ABC Technology Demonstrator Altitude Expansion and Operational Tests," Technical report, Nov 01, 1981.

[20]Padthe, A., Lopez, M., Berger, T., Juhasz, O., Tobias, E., and Glover, E., "Design, Modeling, and Flight Dynamics Analysis of Generic Lift-Offset Coaxial Rotor Configurations," , 05 2022.
doi: 10.4050/F-0078-2022-17580

[21]Celi, R., "HeliUM 2 Flight Dynamic Simulation Model: Developments, Technical Concepts, and Applications," American Helicopter Society 71st Annual Forum, Virginia Beach, VA, May 2015.

[22]Saetti, U. and Horn, J. F., "Flight Simulation and Control using the Julia Language," Proceedings of the AIAA SciTech Forum, San Diego, CA & Virtual, Jan 3-7, 2022.
doi: https://doi.org/10.2514/6.2022-2354

[23]Kokotovic, P. V., O'Malley, R. E., and Sannuti, P., "Singular Perturbations and Order Reduction in Control Theory, an Overview," *Automatica*, Vol. 12, (2), 1976, pp. 123–132.
doi: https://doi.org/10.1016/0005-1098(76)90076-5

[24]Horn, J. F., "Non-Linear Dynamic Inversion Control Design for Rotorcraft," *Aerospace*, Vol. 6, (38), 2019.
doi: https://doi.org/10.3390/aerospace6030038

[25]Frazzoli, E., Dahlel, M. A., and Feron, E., "Maneuver-Based Motion Planning for Nonlinear Systems With Symmetries," *IEEE Transactions on Robotics*, Vol. 21, (6), Dec 2005, pp. 1077–1091.
doi: https://doi.org/10.1109/TRO.2005.852260

[26]Leishman, J. G., *Principles of Helicopter Aerodynamics*, Cambridge University Press, 2006.

[27]Guner, F., "Hover Performance Predictions of Coaxial Rotor Configurations Using the Updated CMTSVT Multirotor Inflow Model," Proceedings of the 48$^{\text{th}}$ European Rotorcraft Forum, Winterthur, Switzerland, Sep 6–8, 2022.

[28]McRuer, D. T., Ashkenas, I. L., and Graham, D., *Aircraft Dynamics and Automatic Control*, Princeton University Press, Princeton, NJ, 1973, Chapter 6.